

THE FORMATION AND EVOLUTION OF STAR CLUSTERS IN INTERACTING GALAXIES

MOUPIYA MAJI^{1,2}, QIRONG ZHU^{1,2}, YUEXING LI^{1,2}, JANE CHARLTON¹, LARS HERNQUIST³ AND ALEXANDER KNEBE^{4,5}

¹Department of Astronomy & Astrophysics, The Pennsylvania State University, 525 Davey Lab, University Park, PA 16802, USA

²Institute for Gravitation and the Cosmos, The Pennsylvania State University, University Park, PA 16802, USA

³Harvard-Smithsonian Center for Astrophysics, Harvard University, 60 Garden Street, Cambridge, MA, 02138, USA

⁴Departamento de Física Teórica, Módulo 8, Facultad de Ciencias, Universidad Autónoma de Madrid, E-28049 Madrid, Spain

⁵Astro-UAM, UAM, Unidad Asociada CSIC, E-28006 Madrid, Spain

ABSTRACT

Observations of globular clusters show that they have universal lognormal mass functions with a characteristic peak at $\sim 2 \times 10^5 M_\odot$, but the origin of this peaked distribution is highly debated. Here we investigate the formation and evolution of star clusters in interacting galaxies using high-resolution hydrodynamical simulations performed with two different codes in order to mitigate numerical artifacts. We find that massive star clusters in the range of $\sim 10^{5.5} - 10^{7.5} M_\odot$ form preferentially in the highly-shocked regions produced by galaxy interactions. The nascent cluster-forming clouds have high gas pressures in the range of $P/k \sim 10^8 - 10^{12} \text{ Kcm}^{-3}$, which is $\sim 10^4 - 10^8$ times higher than the typical pressure of the interstellar medium but consistent with recent observations of a pre-super star cluster cloud in the Antennae Galaxies. Furthermore, these massive star clusters have quasi-lognormal initial mass functions with a peak around $\sim 10^6 M_\odot$. The number of clusters declines with time due to destructive processes, but the shape and the peak of the mass functions do not change significantly during the course of galaxy collisions. Our results suggest that gas-rich galaxy mergers may provide a favorable environment for the formation of massive star clusters such as globular clusters, and that the lognormal mass functions and the unique peak may originate from the extreme high-pressure conditions of the birth clouds and may survive the dynamical evolution.

Keywords: galaxies: interactions, galaxies: star clusters: general, globular clusters: general, methods: numerical

1. INTRODUCTION

Star clusters (SCs) are building blocks of galaxies, so their origin and evolution are important aspects of the study of galaxy formation. Over the past two decades, numerous young massive clusters (YMCs) have been observed by the Hubble Space Telescope in interacting and merging galaxies, such as NGC 1275 (Holtzman et al. 1992), NGC 7252 (Whitmore et al. 1993), NGC 3921 (Schweizer et al. 1996), NGC 4038/39 or the Antennae Galaxies (Whitmore & Schweizer 1995; Whitmore et al. 1999, 2010), NGC 4449 (Annibali et al. 2011), and NGC 7176/7174 (Miah et al. 2015). The YMCs formed in these environments are compact (\sim few parsecs), gravitationally-bound objects with masses $> 10^4 M_\odot$ and ages $\sim 10 - 100$ Myr (Portegies Zwart et al. 2010). The initial cluster mass function (ICMF) of these young clusters, however, is not well-determined. Some studies suggested that it can be described as a

falling power law with $dN/dM \propto M^{-2}$ (Zhang & Fall 1999; Bik et al. 2003; McCrady & Graham 2007; Fall & Chandar 2012), some argued that it might be better fit by a Schechter function with power index -2 and a characteristic mass of few $10^6 M_\odot$ (Bastian 2008; Portegies Zwart et al. 2010), and some proposed that it is not a power law at all mass scales but has a turnover at the low mass end (Cresci et al. 2005; Anders et al. 2007).

On the other end of the SC spectrum are old globular clusters (GCs) that have been observed extensively in nearby galaxies (e.g., Harris 1991; Brodie & Strader 2006; Gratton et al. 2012; Kruijssen 2014, 2015). These are massive ($\sim 10^4 - 10^6 M_\odot$), gravitationally-bound, compact (few pc) and old (age $\simeq 10 - 13$ Gyr) systems that formed in the early universe and have survived to the present-day (Forbes & Bridges 2010; Vandenberg et al. 2013). It has been widely suggested that YMCs could be progenitors of these globular clusters (de Grijs 2007; Longmore et al. 2014). However, the observed globular cluster mass functions (GCMFs) are bell-shaped or lognormal-shaped with a peak mass

around $1.5\text{--}3 \times 10^5 M_\odot$ (Harris 2001; Jordán et al. 2007), which are remarkably different from those of YMCs.

In order to explain the discrepancy between mass functions of YMCs and GCs, a number of studies have focused on the dynamical evolution of SCs. Some theorized that the GCs were formed from the collapse of protogalactic clouds and these clusters had bell shaped ICMFs to begin with (Fall & Rees 1985; Vesperini 2000, 2001; Parmentier & Gilmore 2007). The more prevalent theory suggested that young GCs start with a power-law ICMF, and during evolution they are affected by a number of destructive processes that can disrupt the lower mass clusters more easily and more frequently than their higher mass counterparts, resulting in a lognormal profile (Gnedin & Ostriker 1997; Baumgardt 1998; Fall & Zhang 2001). Such destruction can rise from two-body relaxation, shock heating, supernova explosions, tidal shocking and stellar dynamical evaporation (e.g., Gnedin et al. 1999a; Fall & Zhang 2001; McLaughlin & Fall 2008). In particular, tidal forces induced by galaxy interactions or GCs passing through a galactic disk can generate efficient heating from strong tidal shocks, which significantly affect the evolution of GCs (Combes et al. 1999; Gnedin et al. 1999a,b).

However, little is known about the formation conditions that determine the mass functions of YMCs and how they are related to those of GCs. It has long been suggested that globular clusters preferentially form in regions with extremely high pressure (Elmegreen & Efremov 1997; Ashman & Zepf 2001). High pressure in molecular clouds can result in high velocity dispersions (several tens of km/s) which lead to larger binding energy. This helps the cloud not to get dispersed by typical HI clouds. With rising pressure, the specific star formation efficiency of the region can increase significantly by up to one order of magnitude (Jog & Solomon 1992; Jog & Das 1996). High binding energy and high specific star formation efficiency are critical to the formation of massive, bound SCs. From the present-day properties of GCs, it is suggested that the cluster-forming clouds should have experienced high pressure on the order of $P/k_B \gtrsim 10^8 \text{ K cm}^{-3}$, which is $\gtrsim 10^4$ times larger than the ambient interstellar medium pressure in our galaxy (Jenkins et al. 1983; Boulares & Cox 1990; Elmegreen & Efremov 1997; Welty et al. 2016). However, these extreme pressures can be easily produced in interacting galaxies by violent shocks, so they are theoretically expected to be ideal formation sites for GCs.

On the observational front, it has been difficult to directly observe the physical conditions of a proto super-star cluster cloud (SSC - star clusters with the possibility of evolving into GCs). Wei et al. (2012) observed molecular cloud regions in the Antennae Galaxies and found very massive ($\gtrsim 10^6 M_\odot$) clouds in the centers of

high star formation regions with large velocity dispersion. Recently, Johnson et al. (2015) have studied the properties of a pre-SSC cloud in the merging galaxies of the Antennae in detail via CO observations. This cloud is not yet forming stars, but is expected to begin doing so in less than 1 Myr, which makes it an ideal candidate to investigate SSC formation conditions. Direct measurements of the cloud suggest that it has mass of $> 5 \times 10^6 M_\odot$ and a radius of ~ 25 pc which falls in the range of GC properties. The cloud is experiencing a tremendously high external pressure $P/k_B > 10^8 \text{ K cm}^{-3}$. Adamo et al. (2015) studied the SCs in M83 at different radii from the galaxy center and concluded that high gas pressure increases cluster formation efficiency.

In order to investigate the formation and evolution of SCs and their mass functions, we need realistic simulations of galaxies with SC systems to understand the complex interplay of all the creation and destruction processes. However, due to the large dynamical range (from sub pc for star formation to kpcs for galaxies), mass scale (from star clusters of $\sim 10^4 M_\odot$ to galaxies of $10^{12} M_\odot$), and the various physical processes involved (cluster formation in GMCs, stellar evolution, binary interaction, shocks, tidal disruptions etc), it has been a challenge to study formation and evolution of SCs in galaxies numerically. Most of the early simulation efforts assumed a shape for the ICMF, generally power laws or Schechter functions, and then simulated their evolution using N-body codes (Vesperini & Heggie 1997; Baumgardt & Makino 2003; Lamers et al. 2010). Some simulations have focused on particular aspects of the problem, such as the evolution of GCs in the tidal fields of mergers (Renaud & Gieles 2013), star escape rate from GCs (Gieles & Baumgardt 2008) and the effects of intermediate mass black holes on GCs (Lützgendorf et al. 2013). A few simulations explore SCs in specific environments such as high redshift galaxies (Prieto & Gnedin 2008) and dwarf galaxies (Kruijssen & Cooper 2012). Some variants of N-body simulations have also been applied, for example, Renaud et al. (2011) used a tensor field to describe tidal fields.

It is very important to include hydrodynamics of the gas in the galaxy to fully understand SC formation and evolution, but it can be highly computationally expensive to explore the entire range of processes. For example, Li et al. (2004) used sink particles to represent SCs in high-resolution, smoothed particle hydrodynamics (SPH) simulations but could not follow the structure of clusters; Kruijssen et al. (2011, 2012) used N-body/hydro simulations for the galaxies but followed the cluster evolution semi-analytically. A more complete treatment of galaxy simulation and SC identification emerged recently. Renaud et al. (2015) modeled an Antennae-like merger using an adaptive mesh refine-

ment (AMR) grid-based code and identified SCs with a friends-of-friends (FOF) group finding algorithm. They found that the cluster formation rate roughly follows the star formation rate, and that clusters formed in interacting galaxies are up to 30 times more massive than those formed in isolated galaxies. However, a detailed study of the formation conditions of SCs and the evolution of cluster mass functions is needed.

In this study, we perform fully hydrodynamic simulations of galaxy mergers using two different codes: GADGET (Springel et al. 2001; Springel 2005) and GIZMO (Hopkins 2015). We identify the SCs in them as overdense groups of bound particles, using the Amiga Halo Finder (AHF¹, Gill et al. 2004; Knollmann & Knebe 2009). We investigate the physical conditions of SC formation by tracking the properties of the nascent birth clouds. We follow the early evolution of their mass function to understand the connection between YMCs and GCs and the origin of the mass function peak of GCs. This is one of the first studies to realistically identify SCs and follow their formation and evolution in galaxy mergers.

Our paper is organized as follows: in § 2 we describe the methods, which include the numerical codes, galaxy model and cluster identification; in § 3 we present the results of cluster formation and physical conditions, and the initial cluster mass functions; in § 4 we explore the evolution of cluster mass functions; in § 5 we discuss the limitations of our study; and we summarize our findings in § 6.

2. METHOD

In this study, we perform hydrodynamical simulations of a galaxy merger of two Milky Way-size progenitors using two different hydrodynamics codes: the improved SPH code GADGET developed by Springel et al. (2001) and Springel (2005), and the new meshless code GIZMO developed by Hopkins (2015). In order to reduce numerical artifacts on the physical results, we have implemented the same physical processes in both codes, and use the same initial conditions in the simulations. The SCs are identified in the simulations using a density-based group finding algorithm Amiga Halo Finder (AHF, Knollmann & Knebe 2009; Gill et al. 2004). In what follows we briefly describe the codes, galaxy model and SC identification used in the simulations; we refer the reader to read the references therein for detailed descriptions.

2.1. Hydrodynamic Codes

GADGET (Springel et al. 2001; Springel 2005) is a massively parallel N-body/SPH code. It handles the components of a galaxy in two distinct ways: it treats the motions and evolution of dark matter and stars as collisionless particles in an N-body problem, while the gas is dealt with using the SPH method (Gingold & Monaghan 1977; Hernquist & Katz 1989). The N-body particles are described by the collisionless Boltzman and Poisson equations, and the hydrodynamics of the fluid is followed using properties of neighboring gas particles smoothed by a kernel function. The gravitational force of each particle is calculated with a tree algorithm in which particles are grouped together and their effect is taken as a single multipole force, which reduces the computation cost greatly to $O(N \log N)$ compared to the direct summation of each particle pair with complexity $O(N^2)$. In this code, an artificial viscosity term is introduced into the equation of motion of SPH to represent the viscosity which often arises in ideal gases due to shocks caused by microphysics. The GADGET-2 we use explicitly conserves energy and entropy in the SPH formulation (Springel & Hernquist 2002). This version and its variants have been widely used in a large number of applications, from large-scale cosmological simulations (e.g., Springel & Hernquist 2003b; Springel et al. 2005b; Feng et al. 2013; Schaye et al. 2015) to galaxy mergers (e.g., Springel 2000; Li et al. 2004; Springel & Hernquist 2005; Hopkins et al. 2005, 2006, 2008; Li et al. 2007; Cox & Loeb 2008; Hayward et al. 2014).

GIZMO (Hopkins 2015) is a new Lagrangian code developed to circumvent the many problems encountered by SPH methods (Agertz et al. 2007; Bauer & Springel 2012; Vogelsberger et al. 2012; Sijacki et al. 2012; Kereš et al. 2012; Nelson et al. 2013; Zhu et al. 2015; Zhu & Li 2016). It derives the hydrodynamic equations using a kernel function to partition the volume, and a Riemann solver to evolve the equations at the Lagrangian face comoving with the mass. GIZMO implements strict conservation of mass, energy and linear and angular momentum and it does not require any artificial diffusion terms to deal with shocks, embodying the advantages of both SPH and grid-based methods. It captures the instabilities of fluid mixing well, greatly reduces numerical noise and artificial viscosity and as a result calculates fluid physics at smaller Mach number more accurately. GIZMO treats the contact discontinuities and shocks more precisely and more efficiently, generally within one kernel length instead of 2-3 as in GADGET, and it does not have the zeroth order and first order errors that are present in SPH (Zhu et al. 2015), so it can attain higher accuracy with a much smaller number of neighbors which results in a faster convergence. We have used the meshless finite-mass mode of Gizmo for our project. The mass of an individual gas element is conserved in this

¹ The AHF code is available at <http://popia.ft.uam.es/AHF/Download.html>

mode, which allows us to trivially trace the history of star particles to their progenitor gas particles (otherwise, one needs tracer particles to do so).

A detailed comparison between GADGET and GIZMO in galaxy simulations has been conducted by [Zhu & Li \(2016\)](#), who showed a general agreement between the two simulations but there were notable differences in a number of galaxy properties such as star formation history, gas fraction and disk structures.

In this study, our motivation for using these two codes to perform the same merger simulation is to reduce the possibility of numerical artifacts affecting our results. As we will show in § 3, although the detailed star formation history of the mergers is different between the two simulations, the overall distribution functions of the cluster mass and the pre-cluster gas pressure agree well, which suggests that our results are physical and robust, because we can argue against the effects of numerical artifacts such as the number of neighbors and artificial viscosity on these results.

2.2. Galaxy Model

Our simulations consider major mergers of two equal-mass Milky Way - sized galaxies. The galaxy is constructed using the model of [Mo et al. \(1998\)](#), which has a dark matter halo with a Hernquist density profile ([Hernquist 1990](#)), a thin disk with gas and stars, and a black hole in the center. The galaxy properties are similar to those of the Milky Way: the total mass is $10^{12} M_{\odot}$, the gas fraction $f_{\text{gas}} = 0.2$, the radial scale length of the galaxy is 3 kpc, and the disk height is one-fifth of it. The disk contains 4% of its total mass, and the seed mass of the black hole is $10^5 M_{\odot}$.

The interstellar medium (ISM) in these galaxies is modeled using a sub-grid multi-phase recipe, and the star formation rate follows the empirical Schmidt-Kennicutt law ([Schmidt 1959](#); [Kennicutt 1998](#)) where the surface density of star formation is related to the surface density of gas ($\Sigma_{\text{SFR}} \propto \Sigma_{\text{gas}}^{1.4}$). The radiative cooling and heating in the ISM is modeled with the assumption that the medium is in collisional equilibrium and there is an external UV background ([Haardt & Madau 1996](#)). We have also followed feedback processes from both supernovae ([Springel & Hernquist 2003a](#)) and active galactic nuclei ([Springel et al. 2005a](#)). Supernova feedback includes thermal energy and galactic winds. The wind energy efficiency is 5% of the supernovae energy, and the wind direction is anisotropic: winds carry energy and matter perpendicular to the disk plane. The feedback from the black holes is in the form of thermal energy deposited isotropically into the surrounding gas.

We note that [Renaud et al. \(2015\)](#) have performed a simulation of Antennae-like merger. In order to explore a more extreme merger environment, we simulate

a head-on collision of two Milky Way-sized galaxies, in which the progenitors are initially placed on a parabolic orbit with the inclination of both with respect to the orbital plane as $\theta = 0$ and $\phi = 0$. In the simulations, each galaxy is initially started with 82,000 gas particles, 328,000 star particles and 1,476,860 dark matter particles, which yield a mass resolution of $5 \times 10^4 M_{\odot}$ for the gas and star particles, and $6 \times 10^5 M_{\odot}$ for each dark matter particle.

2.3. Star Cluster Identification

Finding groups or structures in a given set of data is a classic problem in data mining. There are many algorithms for group finding, which essentially differ in their notion of groups and in their methods. The two main classes are particle-based and density-based algorithms. The most widely used method of group finding in astronomy is the FOF algorithm ([Davis et al. 1985](#)). It is a particle-based algorithm where all particles within a given linking length are considered as a group. However, there are two significant downsides of this approach even with an adaptive linking length ([Suginohara & Suto 1992](#)): i) if two groups have a linking bridge, they will be identified as one group; ii) it cannot identify substructures within a structure.

The other class of group-finding algorithms is density-based, which identify overdensities in the field as groups ([Warren et al. 1992](#); [Bertschinger & Gelb 1991](#); [Klypin & Holtzman 1997](#); [Gill et al. 2004](#)). These methods do not suffer from the problems of the FOF methods described above. For this reason, we adopt the density-based hierarchical group finding algorithm AHF ([Knollmann & Knebe 2009](#)) to identify SCs in the simulations using the following procedures.

First, AHF divides the simulation box into grid regions. It determines the density inside each grid cell and compares the density to a threshold or background density value. If the computed density exceeds the threshold, it divides the grid into half of its initial size. It computes the densities in each of the refined grid cells and again compares with the threshold. This process goes on recursively until all the cells in the simulation box have densities less than the threshold value. Next, it starts from the finest grid and marks isolated overdense regions as possible clusters. It goes on to the next coarser level and again identifies possible regions as clusters. Importantly, it links the possible clusters in finer grids to their respective coarser parts (linking daughters to parents). This continues until it has reached the coarsest grid and finally it builds a tree of clusters with subclusters.

Considering the observed physical properties of young massive clusters, we impose a few criterions on the groups identified by AHF to qualify them as SCs. Each

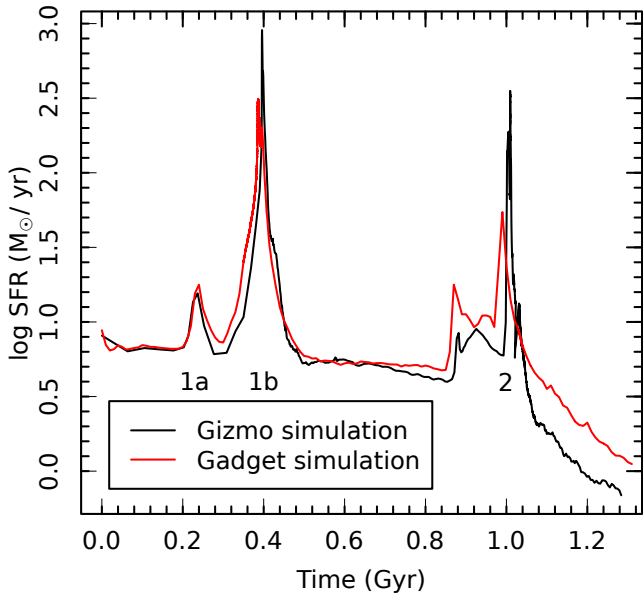


Figure 1. The star formation histories of galaxy mergers in both GIZMO (black curve) and GADGET (red curve) simulations. Both simulations show two starburst episodes during the close encounters of the two galaxies, at times $\sim 0.2 - 0.45$ Gyr and $\sim 0.8 - 1.1$ Gyr, respectively. In order to investigate the triggering source of star formation, we calculate gravitational torques on star forming gas during three star formation peaks as labeled: minor peak 1a at 0.23 Gyr and major peak 1b at 0.4 Gyr during the first close passage, and major peak 2 at 1 Gyr during the final coalescence, and show the results in Figure 3.

group should be gravitationally bound and have no substructures in order to only include individual star clusters. It should contain stars and have at least 4 baryonic particles, which means the minimum cluster mass is $2 \times 10^5 M_\odot$. The upper limit of group mass is set at $10^8 M_\odot$, and the baryonic fraction (mass ratio of baryons to dark matter) of each group should be larger than unity in order to distinguish the star clusters from dwarf galaxies that may form in our simulations. Such an approach provides a holistic identification of star clusters in our study.

3. FORMATION OF STAR CLUSTERS

3.1. Starbursts in Interacting Galaxies

In the simulations, the progenitor galaxies start moving towards each other at $t = 0$ on a parabolic orbit. They have their first close encounter at $t \sim 0.23$ Gyr, and the second one at $t \sim 0.9$ Gyr until the final coalesce at $t \sim 1$ Gyr. During the close passages, vigorous star formation is triggered by the compression of gas by tidal forces and rising gas densities in the inner region of the galaxies due to gravitational torques (Barnes & Hernquist 1991, 1996). As shown in Figure 1, the first

starburst occurs at $t \sim 0.2 - 0.5$ Gyr, when the star formation rate (SFR) increases by nearly two orders of magnitude and reaches a peak of $\sim 10^3 M_\odot/\text{yr}$ at $t \sim 0.4$ Gyr. The second starburst takes place at $t \sim 0.9 - 1.1$ Gyr, and the SFR peaks at $\sim 10^2 M_\odot/\text{yr}$ at $t \sim 1$ Gyr.

The star formation history of galaxy mergers depends strongly on the progenitor properties and orbital parameters. The SFR in our simulation is higher than typical mergers at the local universe. Renaud et al. (2015) estimated from their simulation that the SFR of Antennae merger at its starburst phase is $\sim 10^2 M_\odot$. However, star formation in ultra-luminous infrared galaxies (ULIRGs) in nearby universe can have comparable intensity. For example, radio recombination line studies of merger driven starburst galaxy Arp 220 (77 Mpc away) suggest a mean SFR of $\sim 240 M_\odot/\text{yr}$ or more plausibly short periods of intense starbursts with SFR of $\sim 10^3 M_\odot/\text{yr}$ (Anantharamaiah et al. 2000; Thrall 2008; Varenus et al. 2016). We note that the mass of Arp220 is estimated as $\sim 10^{10} M_\odot$ (Scoville et al. 1997), much lower than our modeled galaxies. The high SFR in our simulated galaxies may be a product of both their high mass progenitors and their extreme orbital parameters with the head-on collision.

As demonstrated in Figure 1, there is a remarkable difference in the star formation histories between the two simulations in that GIZMO produces higher SFR peaks than GADGET by a factor of 3 – 5. This is due to the more accurate treatments of fluids and shocks in GIZMO. Similar differences have also been seen in the code comparison study of galaxy mergers using GADGET and the moving-mesh code AREPO by Hayward et al. (2014), who reported that AREPO produces higher SFRs than GADGET by up to a factor of 10 for mergers of Milky Way - size galaxies.

The strong compression and shocks produced by the galaxy interaction fuel rapid formation of SCs during the starbursts. As demonstrated in Figure 2, most of the SCs form in the nuclear regions of the two merging galaxies, with a few spread in the tidal tails and the galactic bridges. Similar distributions of YMCs have also been observed in galaxy mergers, including nuclear region clusters by Whitmore & Schweizer (1995); Miller et al. (1997), and tidal tail clusters by Barnes & Hernquist (1992); Knierman et al. (2003); Bastian et al. (2005); Mullan et al. (2011).

In order to investigate the triggering source of star formation during the merging process, we track the gas particles that form stars at the three star formation peaks, minor peak 1a at 0.23 Gyr and major peak 1b at 0.4 Gyr during the first close passage, and major peak 2 at 1 Gyr during the final coalescence, as labeled in Figure 1. It was shown by Hernquist (1989) that the major star formation episodes in galaxy mergers are marked

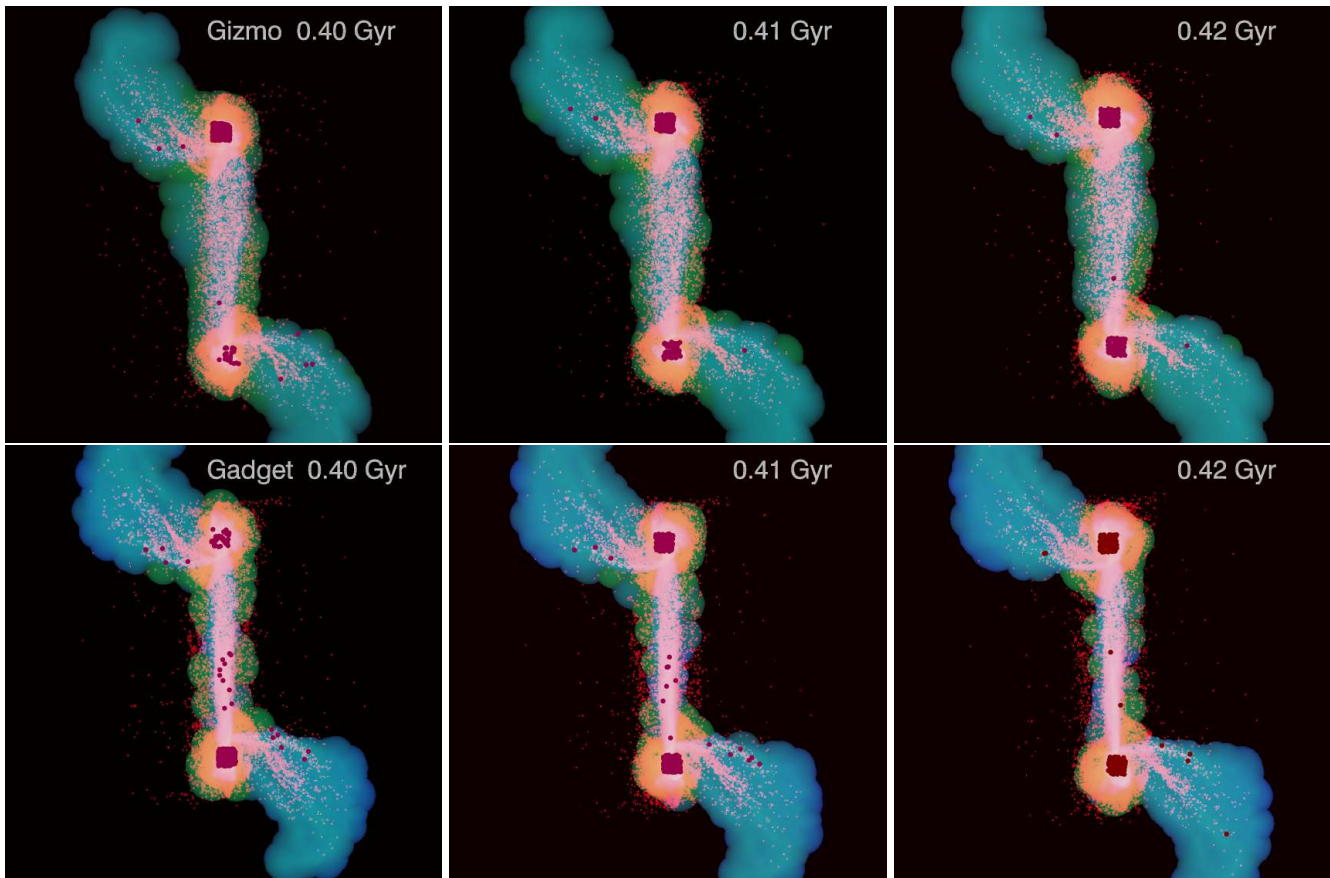


Figure 2. Snapshots of the galaxy merger at three different times, 0.40 Gyr, 0.41 Gyr and 0.42 Gyr during the first starburst phase when most clusters form, from both GIZMO (top panels) and GADGET (bottom panels) simulations. The images are projected gas density maps color-coded by gas temperature (the colors from blue to red indicates hotter gas, the brightness from dark to white measures increasing density). The red dots are stars, and the filled maroon circles represent newly formed star clusters. The maroon region in the center of each galaxy indicates overlapping star clusters. The box length is 100 kpc in physical coordinates.

by a rapid loss of the angular momentum of the star forming gas driven by the gravitational torque. We follow the procedure of [Barnes & Hernquist \(1996\)](#) and calculate the gravitational torque, $\tau = r \times F$, exerted on these star-forming gas particles by the gas and stars in the same galaxy (internal torque), and by gas, stars and halo particles of the other galaxy (external torque). As shown in [Figure 3](#), the internal torque is higher than the external counterpart by orders of magnitude for all tracked star-forming gas particles during the galaxy interaction. Similar results have been reported by a number of theoretical studies of major mergers (e.g. [Hernquist 1989](#); [Mihos & Hernquist 1994](#); [Barnes & Hernquist 1996](#); [Hopkins et al. 2009](#)), which show that the internal torque is the dominant source of torque that drives the loss of angular momentum in these interacting galaxies. The close encounter of the galaxies produces strong tidal forces that results in a non-axisymmetric response in the galaxy disks. These forces deform the galaxy disks and form gaseous and stellar bars in the galaxies. These gas bars lead the stellar bars by a few de-

grees ([Barnes & Hernquist 1991](#)) which eventually produces a strong torque on the gas near the center that drives rapid gas inflow towards the nuclear region, resulting in vigorous starburst. From [Figure 2](#), the majority of clusters formed at the starburst phase are highly clustered in the center region of each galaxy, indicating their origin from the nuclear gas inflow, while the few clusters formed in the bridge and tidal tails may be triggered by tidal force, as suggested by [Renaud et al. \(2009\)](#) and [Renaud et al. \(2014\)](#).

We note that the first major star formation peak 1b (at 0.4 Gyr) takes place about 160 Myr after the first close pericentric passage at ~ 0.24 Gyr. Similar time delay has been found in other simulations of galaxy mergers (e.g., [Mihos & Hernquist 1994, 1996](#); [Cox & Loeb 2008](#); [Hayward et al. 2014](#)), as the timescale to build up the gas density driven by internal torque for star formation. In addition, we note that there is a minor star formation peak of $\sim 15 M_{\odot}/\text{yr}$ at 1a (0.24 Gyr) preceding the the major one of $\sim 800 M_{\odot}/\text{yr}$ at 1b (0.4 Gyr). We find that the ratio of external to internal torque peaks

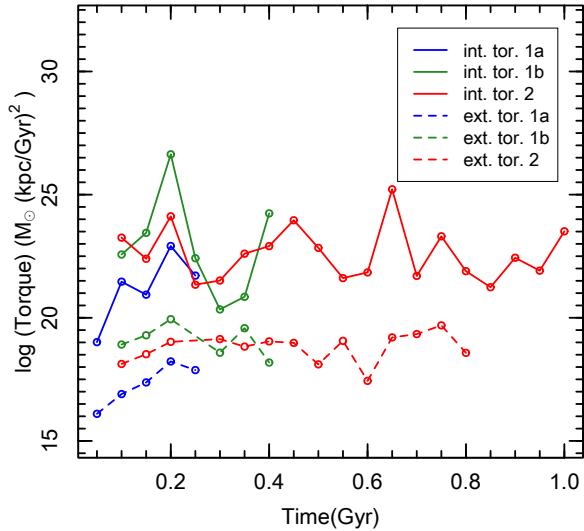


Figure 3. Evolution of the gravitational torques on the gas particles that eventually form stars during the three star formation peaks, 1a (at time 0.23 Gyr, *blue*), 1b (at 0.4 Gyr, *green*), and 2 (at 1 Gyr *red*), as labeled in Figure 1. The solid and dashed lines represent internal and external torques, respectively. Note that during the final coalescence at time $\sim 0.8 - 1.1$ Gyr, only internal torque is available.

during the 1a phase, suggesting that external torque from tidal force may contribute to the star formation as well. Studies by Renaud et al. (2009, 2014) have shown that tidal force during galaxy interaction may compress the gas and enhance the star formation.

3.2. Initial Cluster Mass Functions

The resulting mass functions of the SCs formed during the first close encounter are shown in Figure 4. Although the total number of clusters in the same snapshot differs between the GIZMO and GADGET simulations by a factor of ~ 1.3 , the range of $\sim 150 - 200$ is in good agreement with observations of galaxy mergers such as the Antennae (Whitmore et al. 1999; Larsen 2010). More interestingly, both simulations produce similar mass distributions which resemble a peaked or a quasi-lognormal function, with a GIZMO peak around $10^{5.8-6} M_{\odot}$ and the GADGET peak at $10^{6-6.2} M_{\odot}$.

Our mass functions do not show a purely declining power law, as suggested by many observations of YMCS (e.g., Zhang & Fall 1999; Bik et al. 2003; McCrady & Graham 2007; Fall & Chandar 2012). This could be due to the limited resolution in our simulation so we cannot resolve clusters at mass lower than $10^5 M_{\odot}$. However, Renaud et al. (2015) also reported lognormal-shape ICMFs from their Antennae simulation even though they have a much higher mass resolution ($\sim 70 M_{\odot}$). It is also possible that the power-law phase is extremely

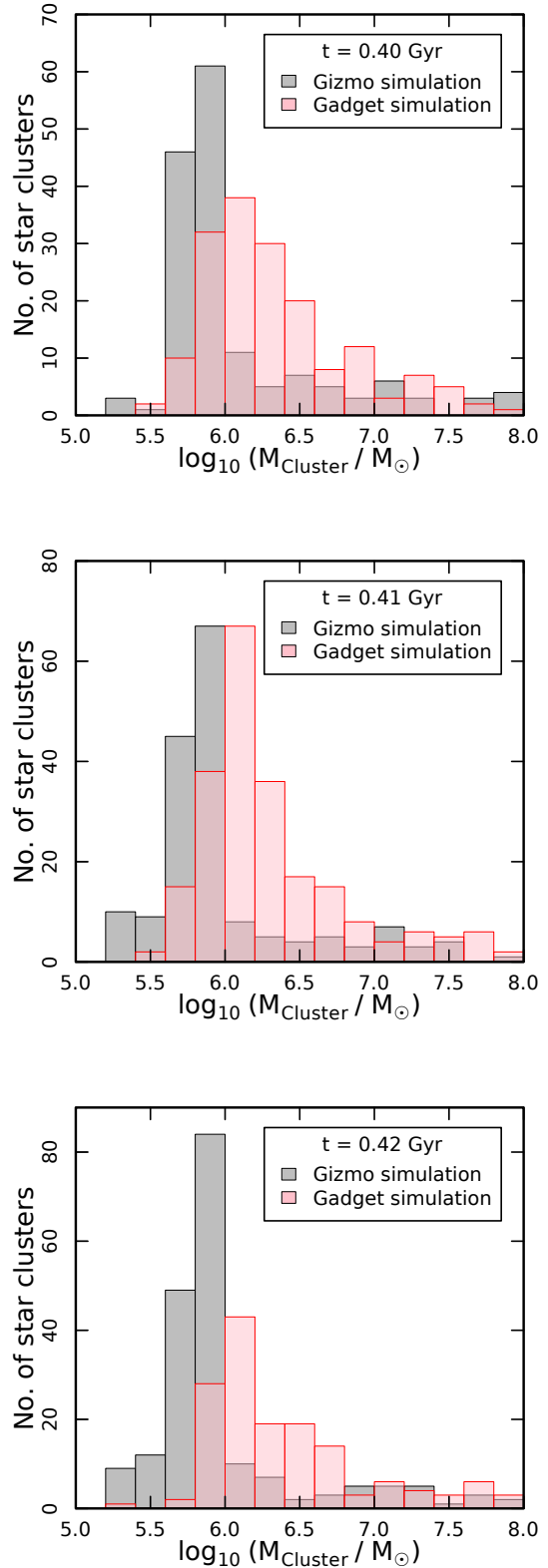


Figure 4. Mass functions of star clusters formed at 0.40 Gyr, 0.41 Gyr and 0.42 Gyr during the first starburst phase when most clusters form, from both GIZMO (grey) and GADGET (red) simulations. The total number of clusters in the three snapshots from GIZMO (GADGET) simulation is 158 (170), 171 (221), and 197 (151), respectively.

short lived (< 10 Myr) in violent mergers and our snapshot interval (every 10 Myr) misses that phase. We note, however, some observations have suggested that the power law ICMF for YMCs is not universal, rather they have a turnover at low mass (Cresci et al. 2005; Anders et al. 2007).

The peak masses of these ICMFs are higher than those of the observed GCMFs, $\sim 1.5 - 3 \times 10^5 M_\odot$, but it can be predicted that after an evolution of Gyrs, stellar evolution, tidal stripping and other disruptive processes will cause them to lose some of their mass (Kruijssen 2015; Webb & Leigh 2015). We discuss their evolution in more detail in §4. It is encouraging that both of our simulations, together with that by Renaud et al. (2015), produce similar quasi-lognormal ICMFs with similar peak positions, despite having vastly different hydrodynamic solvers, feedback processes and numerical resolutions. This agreement suggests that the lognormal mass function is unlikely due to numerical artifacts but has a physical origin, which will be investigated in the next section.

3.3. Physical Conditions of Cluster Formation and Origin of Lognormal Cluster Mass Functions

In order to explore the physical origin of the quasi-lognormal ICMFs in Figure 4, we examine the physical conditions of cluster formation. As mentioned in § 1, massive SCs form in molecular clouds with very high gas pressures (Elmegreen & Efremov 1997; Ashman & Zepf 2001). When a star-forming cloud is under high pressure, the efficiency of star formation increases and the gas velocity dispersion becomes higher, which in turn help to keep the cloud bound (Jog & Solomon 1992). These physical conditions create an ideal nursery to form massive, gravitationally-bound clusters. Recently, Zubovas et al. (2014) performed an N-body simulation of a molecular cloud and concluded that high external pressures drive efficient star formation and can cause cloud fragmentation, leading to the formation of star clusters. Quantitatively, the external pressure P on a nascent molecular cloud is given by Elmegreen (1989):

$$P = \frac{3\Pi M_{\text{cloud}} \sigma_v^2}{4\pi r^3} \quad (1)$$

where M_{cloud} is the mass of the cloud, σ_v is the velocity dispersion and r is the size of the cloud. The factor Π is given by the ratio of density at the cloud edge and the average density, $\Pi = n_e / \langle n_e \rangle$. This Π ratio is dependent on the density profile of the parent molecular cloud. Locally the probability distribution function of ISM density due to turbulence can be approximated as lognormal but at high density regions ($> 10^3 \text{ cm}^{-3}$), such as at the center of molecular cloud, density profile can develop a power law tail. At these dense places the Π value can be $\gg 1$ and consequently it can increase

the amount of gas above a density threshold which facilitates further star formation (Elmegreen 2011; Renaud et al. 2014).

Elmegreen & Efremov (1997) estimated that the pressure in the birth clouds of typical GC progenitors or SSCs is $\gtrsim 10^8 \text{ K cm}^{-3}$, which is $\gtrsim 10^4$ times higher than the ISM pressure in the Milky Way (Jenkins et al. 1983; Boulares & Cox 1990; Welty et al. 2016).

In the simulations, in order to determine the pressure of the clouds from which the SCs form, we track the cluster members back in time. We take the constituent star particles of a cluster and identify the gas particles from which they formed. We then measure the velocity dispersion of these gas particles and approximate the gas cloud radius as the average distance from gas particles to the center of mass of the cloud. Due to the limited spatial and mass resolutions, we cannot directly probe the cloud density profile for estimating Π , so we approximate $\Pi = 0.5$ following Johnson et al. (2015). We note that realistically Π can be higher, but it would increase all our pressure measurements similarly. With these parameters, we can then calculate the cloud pressure using Equation 1. In Figure 5, we show the resulting pressure distributions against the cluster mass distributions, in comparison with the pressure of a pre-SSC cloud observed in the Antennae by Johnson et al. (2015). We also calculate the pressures of observed SCs in the Antennae Galaxies using the velocity and radius data compiled in Portegies Zwart et al. (2010) and Mengel et al. (2002, 2008) for comparison.

As shown in Figure 5, the pre-cluster cloud pressures from both the GIZMO and GADGET simulations fall in the range of $P/k \sim 10^8 - 10^{12} \text{ K cm}^{-3}$, in good agreement with observations of a proto-SSC cloud in Antennae (Johnson et al. 2015), but they are $10^4 - 10^8$ times higher than the typical pressure in the ISM (Jenkins et al. 1983; Boulares & Cox 1990; Welty et al. 2016). Our results support the theoretical expectations that massive SCs form in high-pressure clouds.

Moreover, the pressure distributions have near lognormal-shape profiles in all panels. Such a quasi lognormal-shape pressure distribution may be the cause of the quasi lognormal-shape ICMF. If we assume a certain cluster formation efficiency η (η that varies with galactic environment, from 0.01 in quiescent galaxies to > 0.4 in interacting galaxies, as suggested by Goddard et al. 2010; Kruijssen 2015), then the mass of a SC M_{cluster} may be related to that of the birth clouds M_{cloud} as $M_{\text{cluster}} \propto \eta M_{\text{cloud}}$; then by inverting Equation 1 we get $M_{\text{cluster}} \propto \eta M_{\text{cloud}} \propto \eta P$. This qualitative relation, as can be inferred from Figure 5, suggests that the distribution of cluster mass depends on that of the cloud pressure, so a lognormal pressure distribution may lead to a lognormal mass distribution of the resulting clus-

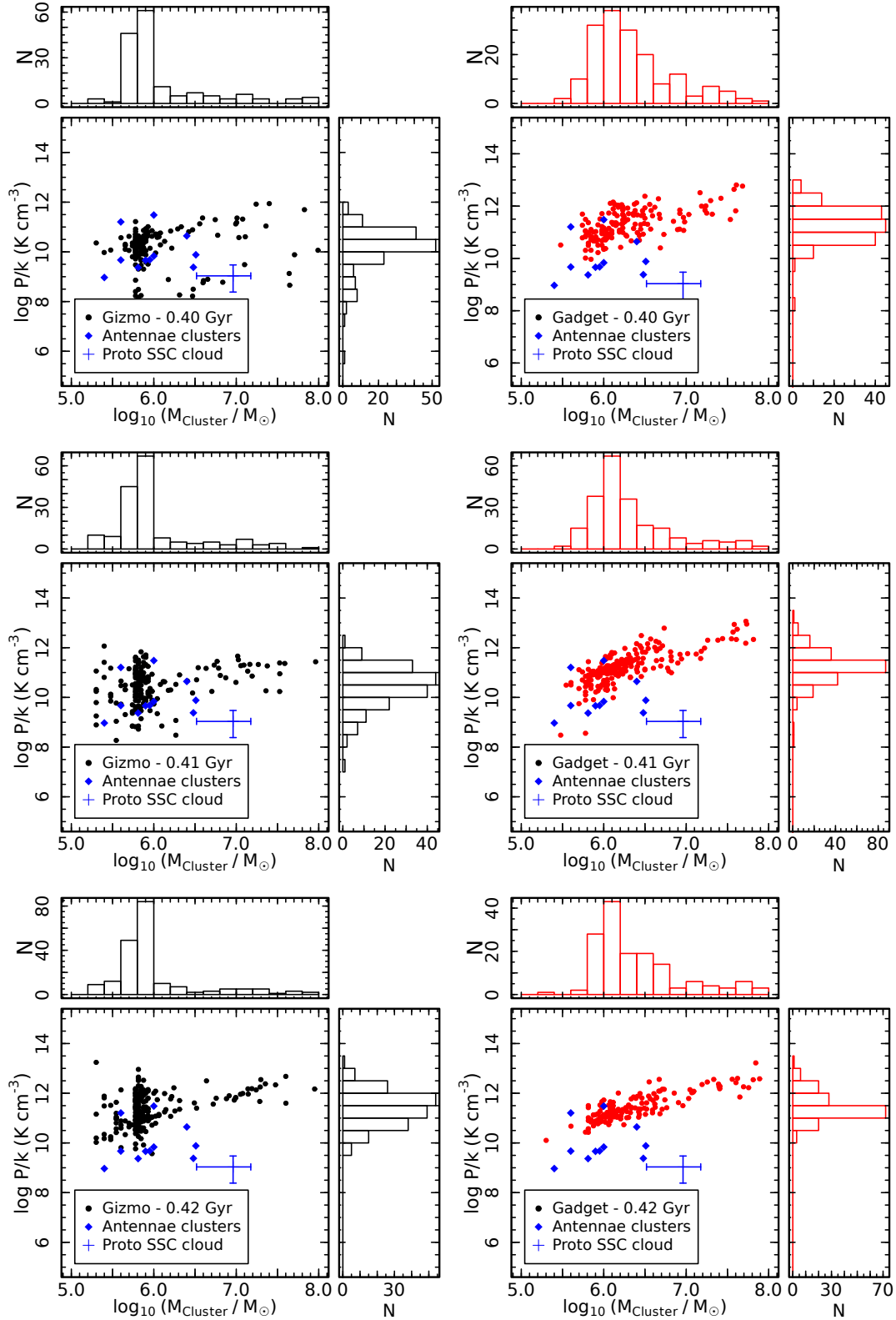


Figure 5. Correlation between pre-cluster gas pressure distributions and initial cluster mass functions at 0.40 Gyr, 0.41 Gyr and 0.42 Gyr during the first starburst phase, when most clusters form, from both GIZMO (black) and GADGET (red) simulations. The pressure derived from the observed pre-super star cluster cloud in the Antennae by Johnson et al. (2015) is represented by the blue cross where the error bars reflect the observational uncertainties in cloud mass ($3.3 - 15 \times 10^6 M_{\odot}$), radius (24 ± 3 pc) and velocity dispersion (49 ± 3 km/s). The pressures derived from observed star clusters in the Antennae using velocity and radius data compiled in Portegies Zwart et al. (2010) and presented by Mengel et al. (2002, 2008) are represented by blue diamonds. The pressure is expressed as P/k where k is the Boltzman constant.

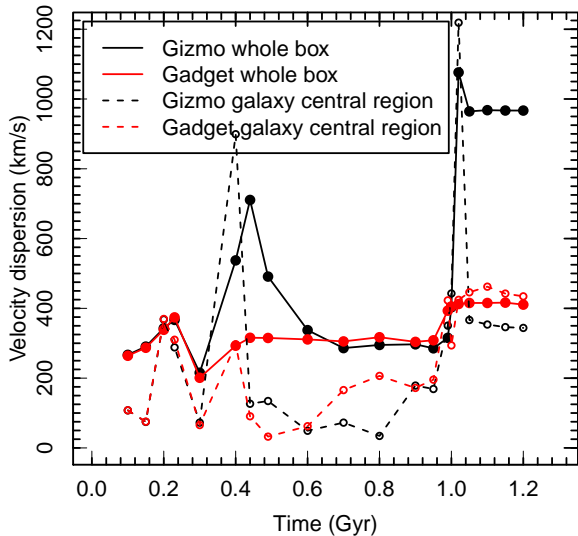


Figure 6. Evolution of the total velocity dispersion of gas and stars in the central region of one galaxy ($5 \times 5 \times 5 \text{ kpc}^3$) (dashed) and the entire simulation box (solid) from both Gizmo (black) and Gadget (red) simulations, respectively.

ters.

Furthermore, Figure 5 also shows that the pressure profiles have a peak at cluster mass around $10^{5.8-6} M_{\odot}$ in the GIZMO simulation and around $10^{6-6.2} M_{\odot}$ in the GADGET simulation, which are exactly the same peaks of their corresponding mass functions. This striking correlation may explain the preferred mass range around the characteristic peak $10^6 M_{\odot}$, as determined by the cloud pressure, for the newly formed SCs in galaxy mergers.

In order to understand the possible physical processes behind the high pressure of the pre-cluster clouds in our simulations, we compare the evolution of the total velocity dispersion of gas and stars in the central region of one galaxy (since the two merging galaxies are identical), i. e., within 5 kpc from the galactic center, and that of the entire simulation box, as shown in Figure 6. We find that the peaks of the total velocity dispersion correspond to those of the star formation as in Figure 1, and that velocity dispersion of the galactic central region is higher than that of the whole box during the major starburst phases at 0.4 Gyr and 1 Gyr. These results suggest that high velocity dispersion around galaxy center, which leads to high pressure, and strong circumnuclear starburst, may result from the same mechanism, compressive shocks driven by gravitational torques during galaxy merger.

Our theoretical findings may provide explanation to a number of observations. In addition to the recent observations of high pressure in a proto-SSC cloud in Antennae (Johnson et al. 2015), measurements of molecular

clouds in the Antennae galaxies have revealed very high velocity dispersion in high star-forming regions (Zhang et al. 2010), which can be explained by compressive shocks (Wei et al. 2012). Herrera et al. (2011) carried out near infrared imaging spectroscopy of the same region and found extended line widths in H_2 emission, which indicates powerful shocks in the region. Similarly, measurements of the CO emission from the starbursting merger of M81 /M82 by Keto et al. (2005) suggest that the molecular clouds undergoing star formation are driven by shock compression. Theoretical studies (Jog & Solomon 1992; Ashman & Zepf 2001) have also shown that during the galaxy encounters, the giant molecular clouds undergo significant shock compression which leads to an increase in the cloud pressure.

We also note that during 1a phase at 0.23 Gyr, the velocity dispersion of the central region is similar that of the whole box, which suggests a spatially extended star formation probably influenced by tidal forces, as discussed in §3.1. Simulation of Antennae galaxies by Renaud et al. (2014, 2015) have shown that compressive tides during the galactic encounter can cause high star formation over extended volumes.

We can see from Figure 5 that the pressures of our simulated clouds are somewhat higher than that of the observed systems. This can arise from the fact that in our simulation the two equal-mass, Milky Way - size galaxies collide mainly head on and merge violently, whereas the Antennae Galaxies have a smaller mass and they are on a milder pericentric passage (Renaud et al. 2015). The extreme conditions in the simulated galaxies produce more powerful shocks which in turn help increase the gas pressure. Such an extreme high-pressure environment may preferentially form massive SCs in a narrow mass range as shown in Figure 4, which may help to explain why we do not see a power-law ICMF in the simulations.

Our simulations bridge the observations and theories of cluster formation and we confirm that massive SCs can form in gas-rich galaxy mergers due to the high gas pressure produced by strong gravitational interactions. Moreover, the special pressure range in such merger environments preferentially forms SCs in a narrow mass interval around the peak mass at $\sim 10^6 M_{\odot}$. Furthermore, the quasi-lognormal pressure distribution may lead to the quasi-lognormal ICMF of SCs formed in colliding galaxies. Our results, therefore, provide clues to the formation of globular clusters and their universal lognormal mass functions, which will be explored in the next section.

4. EVOLUTION OF MASSIVE STAR CLUSTERS

In order to track the change of the cluster mass functions over time, we follow the evolution of the massive

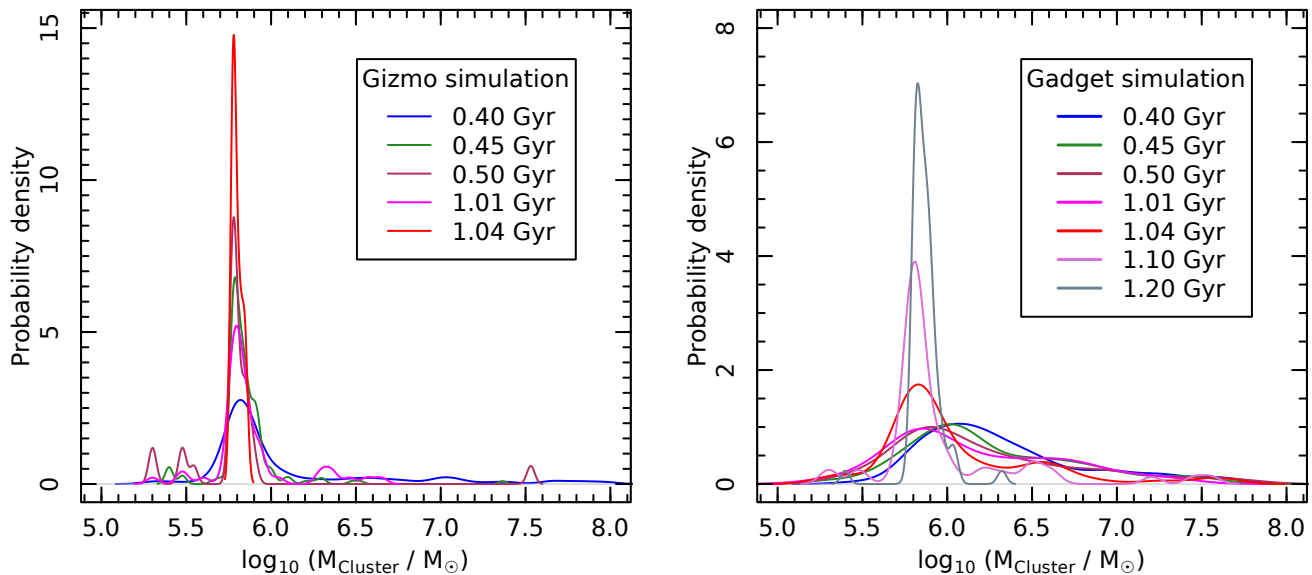


Figure 7. Probability density function of star cluster mass distribution from both GIZMO (left panel) and GADGET (right panel) simulations at different times, as indicated by the different colors. A Gaussian profile is used as the kernel density estimator. The PDFs are normalized such that the area under each curve is unity.

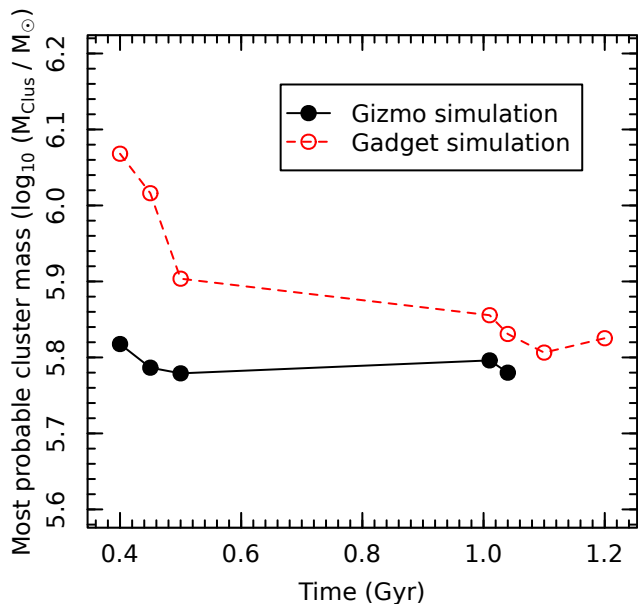


Figure 8. The most probable star cluster mass as a function of time from both GIZMO (black) and GADGET (red) simulations. The data points correspond to the snapshot times in Figure 7.

SCs in our simulations up to 1.3 Gyr when the progenitors completely coalesce. After the initial bursts of star and SC formation during the first close passage at $t \sim 0.2\text{--}0.5$ Gyr, the activity decreases, and many of the clusters are destroyed over time. However, the starburst

activity is renewed again at $t \sim 0.9\text{--}1.1$ Gyr during the final coalescence, although at a lower amplitude than the first burst.

Figure 7 shows the probability density function (PDF) of the cluster mass distribution at different times from both GIZMO and GADGET simulations. Interestingly, the PDFs from the GIZMO simulation have similar narrow profiles, and the position of the peak remains nearly the same over 1 Gyr, while those from the GADGET simulation show a slow evolution from a broad profile to a narrow one and a shift of the peak mass by 0.3 dex over 1 Gyr. The narrowing of the PDF is due to destruction of SCs at both low- and high-mass end by a variety of processes. After ~ 1 Gyr of evolution, about one fourth of the SCs are left, most of them just around the peak mass. The difference in the narrowness of the PDFs from the two simulations is also present in their initial mass functions in Figure 4. This probably stems from the different pressure distributions (Figure 5) owing to different treatments of shocks between GIZMO and GADGET, as discussed in § 2.1.

The peak for each density curve is the value of the most probable mass of the clusters for that time, as shown in Figure 8. The most probable cluster mass in the GIZMO simulation is remarkably consistent at $\sim 10^{5.8} M_{\odot}$ over 1 Gyr, while that of the GADGET simulation changes slightly from $\sim 10^{6.09} M_{\odot}$ at the initial starburst to $\sim 10^{5.8} M_{\odot}$ after 1 Gyr. Since these are isolated merger simulations, it is meaningless to continue the simulations for a longer time, but in a cosmological

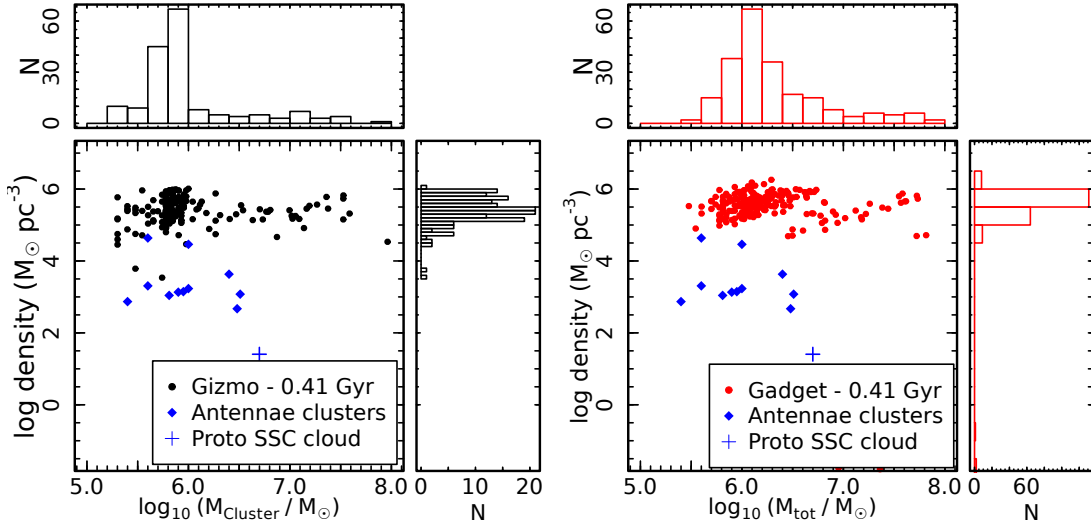


Figure 9. Density of the simulated clusters from both GIZMO (black) and GADGET simulations. The symbols follow the same meaning as described in Figure 5.

context, it can be predicted that the SCs will lose some of their mass due to stellar evolution and other destructive processes. Semi-analytical and N-body simulations by Kruijssen (2015) and Webb & Leigh (2015) found that clusters can lose mass by a factor of 2 – 4 after a Hubble time of evolution. The eventual mass of our simulated clusters can be similar to the observed peak mass of globular clusters at $1.5 - 3 \times 10^5 M_\odot$ (Harris 2001; Jordán et al. 2007).

These results show that the shape of the mass function and the position of the mass peak of massive clusters have little evolution over the course of the galaxy collision of more than 1 Gyr. We note that the evolution of star clusters is subjected to several destructive processes (e.g., Gnedin et al. 1999a; Fall & Zhang 2001). For low-mass clusters ($< 10^5 M_\odot$), the destruction is mainly dominated by two-body relaxation processes, in which the mass of a cluster linearly decreases with time until it is destroyed. For more massive clusters, the evolution is primarily influenced by stellar evolution at early times ($\lesssim 100$ Myr) and by gravitational shocks at later times. These effects are included in our hydrodynamic simulations but the mass resolution is not high enough to resolve the processes realistically, since the two-body relaxation and stellar evolution depend on individual stars. However, the cluster disruption time-scale due to two-body relaxation is proportional to the cluster mass, $t_{rlx} \sim 1.7 \text{ Gyr} \times (M_{clus}/10^4 M_\odot)^{0.62} \times (T/10^4 \text{ Gyr}^{-2})^{-0.5}$, where M_{clus} is the cluster mass and T is the tidal strength around the clusters (Kruijssen et al. 2012). Using the minimum cluster mass of $2 \times 10^5 M_\odot$ in our simulation, and a typical range of tidal strength in the nuclear region (since most of these clusters are concentrated around galaxy nuclei) $T \sim 0.1 - 50 \times 10^{-30} s^{-2}$

(Renaud 2010), we find that the range of the disruption time-scale is $t_{rlx} \sim 4.88 - 108.8$ Gyrs. For more massive SCs, the time-scale is even longer, beyond our run time of 1 Gyr. Therefore, the two-body relaxation may not have a major disruptive effect on these SCs. Furthermore, the mass loss time-scale due to gravitational shocks (t_{sh}) depends strongly on the cluster density, $t_{sh} \sim 3.1 \text{ Gyr} \times \rho/10^4 M_\odot/\text{pc}^3$ (Kruijssen et al. 2012). The majority of our clusters have a density range of $\rho \sim 10^5 - 10^6 M_\odot/\text{pc}^3$, as shown in Figure 9, which suggests $t_{sh} \sim 30 - 300$ Gyrs, much longer than the Hubble time. So gravitational shocks may not have a significant impact on the clusters in our simulation. In addition, as demonstrated by Renaud & Gieles (2013), star clusters formed in galaxy mergers are also affected by the intense tidal field of the galaxies, more so for clusters in the merger remnant compared to the ejected ones. We note, however, the clusters in their simulations have masses $\lesssim 3 \times 10^4 M_\odot$, and mass loss decreases as the cluster mass increases. For example, for a cluster to increase its mass by a factor of 2, from $1.6 \times 10^4 M_\odot$ to $3.2 \times 10^4 M_\odot$, its survival rate (fraction of initial mass survived) after 1 Gyr increases from 0.6 to 0.7. Extrapolating this trend to our clusters which are ~ 10 times more massive than those in Renaud & Gieles (2013), we argue that destruction from tidal fields likely has negligible effects on the clusters we consider here.

Our results suggest that the observed globular clusters may form in high pressure environments induced by galaxy interaction at high redshift when the merger rate was high (e.g., Rodriguez-Gomez et al. 2015; Mistaní et al. 2016). The extremely high gas pressures in the merging environments produce lognormal ICMFs with a peak mass around $\sim 10^6 M_\odot$, and they evolve slowly

over a Hubble time into the universal lognormal profiles with a peak at $\sim 1.5 - 3 \times 10^5 M_\odot$ as observed today.

5. DISCUSSION

We have used the two codes GADGET and GIZMO with significantly different hydrodynamical solvers to simulate the formation and evolution of SCs in galaxy mergers and found similar results. This helps us to reduce the possibility of significant numerical artifacts in our results and suggests that our findings are physical and robust.

In GADGET, the hydrodynamic solver uses a smoothing scheme (Springel 2005), where the physical properties are averaged over a given number of neighboring particles, which is 32 in our simulation. The mass of 32 star particles for our resolution is close to the peak cluster mass seen in the GADGET simulation. However, the GIZMO simulation has no smoothing procedure and the properties do not depend on the number of neighbors but we still see the cluster mass peak at similar masses. This suggests that the peak cluster mass found in our simulation is likely not a numerical artifact, but rather may be a physical feature of SCs formed in such extreme environments. One very potent source of the high pressure in our simulations is the shocks produced during the close passages of galaxies and starburst periods. GIZMO handles shocks much better than GADGET, and it calculates the effects of contact discontinuities more precisely, captures fluid mixing instabilities well and has less numerical noise. These differences are pronounced in Figure 5, where the pressure distribution is more cleanly peaked in GIZMO whereas it is quite spread out in GADGET.

In our simulations, feedback mechanisms from supernovae and active galactic nuclei in the form of thermal energy and galactic winds are included. However, other feedback processes such as photoionization and radiative pressure may affect star formation (Krumholz et al. 2014). On the one hand, high-energy UV photons from OB stars can ionize the HII clouds in ISM, the expanding HII clouds can compress the neutral gas in the outskirts of molecular clouds and the fragmentation of these dense gas can increase the star formation (positive feedback). On the other hand, the momentum imparted on HII gas by ionizing photons can drive gas out of the central regions of GMCs which may suppress star formation or unbind star clusters (negative feedback). Simulations by Dale et al. (2005) show that for very dense clouds (core density $\sim 10^8 \text{ cm}^{-3}$), a highly collimated gas outflow can carry the extra momentum out of the cloud without unbinding the cluster. The photoionization also drives the Jeans mass down, resulting in higher star formation. In the context of star formation in galaxy mergers, comparative studies of merger simulations with and without

these feedback processes by Hopkins et al. (2013) showed that detailed feedback promote more extensive star formation in tails and bridges, but the global star formation properties remain similar. We plan to explore the effects of radiative feedback on the formation and properties of star clusters in a future project.

We have seen from Figure 4 that the ICMF in our simulations does not have the shape of a falling power law, which is commonly observed for many YMC systems. Rather, the ICMF has a quasi-lognormal shape which is preserved in later stages. We doubt that this is due to the limited mass resolution ($5 \times 10^4 M_\odot$) in our simulations, as similar ICMFs were also reported by Renaud et al. (2015), who performed a simulation of the Antennae using a grid-based AMR code with very high mass resolution ($\sim 70 M_\odot$). The agreement among the merger simulations using different codes, various feedback prescriptions and across resolution suggest that the lognormal-shape ICMFs and the unique mass peak are mostly likely special features of clusters formed in the extremely high pressure environments produced by galaxy collisions. In fact, some studies of active galaxies, such as the starburst galaxy NGC 5253 (Cresci et al. 2005) and the interacting Antennae pair (Anders et al. 2007) have shown that the ICMF for YMCs is not a power law for all mass scales, but may rather have a turnover at low mass.

As indicated by Figure 7 and Figure 8, over the evolution of more than 1 Gyr, the mass functions of our star clusters in both the GADGET and GIZMO simulations survives destructive processes and retain the same quasi-lognormal shape with a consistent peak at around $\sim 10^{5.8} M_\odot$. This mass is quite close to the observed GCMF peak at $\sim 1.5 - 3 \times 10^5 M_\odot$. Ideally we would like to have a fully cosmological hydrodynamic simulation of galaxy formation and evolution with a very high mass resolution ($\sim 10^3 M_\odot$) to identify SCs and evolve them for ~ 13 Gyr to explore the fate of the globular cluster mass function, but that remains computationally very expensive. However, the strong trend of survival of the lognormal shape of the ICMFs in our simulations lends support to our speculation that the origin of the lognormal mass functions of the globular clusters may come from the extremely high pressure formation conditions in interacting galaxies.

6. CONCLUSIONS

We have performed high-resolution hydrodynamic simulations of galaxy mergers using two different codes and studied the formation and evolution of SCs in them. We obtained consistent results from both codes, suggesting that our results are physical and robust. Here is a summary of our findings:

- A strong galaxy interaction produces intense shocks and compression of gas, which triggers global starbursts and the formation of massive SCs in the nuclear regions of the mergers and in the tidal bridges and tails. The massive star clusters show quasi-lognormal ICMFs in the range of $\sim 10^{5.5-7.5} M_{\odot}$ with a peak around $10^6 M_{\odot}$.
- The nascent cluster-forming gas clouds have very high pressures in the range of $P/k \sim 10^{8-12} \text{ K cm}^{-3}$, in good agreement with observations and theoretical expectations that massive SCs form in high-pressure environments, which naturally arise in violent galaxy collisions. Moreover, the gas pressures show quasi-lognormal profiles, which suggest that the quasi-lognormal ICMFs of the clusters may be caused by the pressure distributions in the birth clouds. Furthermore, the peak of the pressure distribution correlates with the peak of the cluster mass function at $10^{5.8-6.2} M_{\odot}$, indicating that clusters formed in such extremely high pressure clouds have a characteristic mass around $\sim 10^6 M_{\odot}$.
- The cluster mass functions evolve slowly over time with a declining cluster number due to destructive processes, but the quasi-lognormal shape and the peak of the mass functions do not change significantly during the course of galaxy collisions over 1 Gyr.

Our results suggest that the observed universal lognormal globular cluster mass functions and the unique peak at $\sim 2 \times 10^5 M_{\odot}$ may originate from the high-pressure formation conditions in the birth clouds. Glob-

ular clusters may have formed in extremely high pressure environments produced by violent galaxy interactions at high redshift when mergers were more common. The lognormal cluster mass functions with a preferred most probable cluster mass around $\sim 10^6 M_{\odot}$ may be unique products of such extreme birth conditions, and they evolve slowly over 13 Gyrs but retain the lognormal shape and peak against destructive processes.

ACKNOWLEDGEMENT

We thank Dr. Bruce Elmegreen and Dr. Phil Hopkins for valuable discussions, and Dr. Florent Renaud for his constructive comments which have helped improve the paper significantly. YL acknowledges support from NSF grants AST-0965694, AST-1009867, AST-1412719, and MRI-1626251. AK is supported by the *Ministerio de Economía y Competitividad* and the *Fondo Europeo de Desarrollo Regional* (MINECO/FEDER, UE) in Spain through grant AYA2015-63810-P as well as the Consolider-Ingenio 2010 Programme of the *Spanish Ministerio de Ciencia e Innovación* (MICINN) under grant MultiDark CSD2009-00064. He also acknowledges support from the *Australian Research Council* (ARC) grant DP140100198. We acknowledge the NSF award MRI-1626251 for providing computational resources and services through Institute for CyberScience at The Pennsylvania State University that have contributed to the research results reported in this paper. The Institute for Gravitation and the Cosmos is supported by the Eberly College of Science and the Office of the Senior Vice President for Research at the Pennsylvania State University.

REFERENCES

- Adamo, A., Kruijssen, J. M. D., Bastian, N., Silva-Villa, E., & Ryon, J. 2015, *MNRAS*, 452, 246
- Agertz, O., Moore, B., Stadel, J., Potter, D., Miniati, F., Read, J., Mayer, L., Gawryszczak, A., Kravtsov, A., Nordlund, Å., Pearce, F., Quilis, V., Rudd, D., Springel, V., Stone, J., Tasker, E., Teyssier, R., Wadsley, J., & Walder, R. 2007, *MNRAS*, 380, 963
- Anantharamaiah, K. R., Viallefond, F., Mohan, N. R., Goss, W. M., & Zhao, J. H. 2000, *ApJ*, 537, 613
- Anders, P., Bissantz, N., Boysen, L., de Grijs, R., & Fritze-v. Alvensleben, U. 2007, *MNRAS*, 377, 91
- Annibali, F., Tosi, M., Aloisi, A., & van der Marel, R. P. 2011, *AJ*, 142, 129
- Ashman, K. M., & Zepf, S. E. 2001, *AJ*, 122, 1888
- Barnes, J. E., & Hernquist, L. 1992, *Nature*, 360, 715
- . 1996, *ApJ*, 471, 115
- Barnes, J. E., & Hernquist, L. E. 1991, *ApJL*, 370, L65
- Bastian, N. 2008, *MNRAS*, 390, 759
- Bastian, N., Hempel, M., Kissler-Patig, M., Homeier, N. L., & Trancho, G. 2005, *A&A*, 435, 65
- Bauer, A., & Springel, V. 2012, *MNRAS*, 423, 2558
- Baumgardt, H. 1998, *A&A*, 330
- Baumgardt, H., & Makino, J. 2003, *MNRAS*, 340, 227
- Bertschinger, E., & Gelb, J. M. 1991, *Computers in Physics*, 5, 164
- Bik, A., Lamers, H. J. G. L. M., Bastian, N., Panagia, N., & Romaniello, M. 2003, *A&A*, 397, 473
- Boulares, A., & Cox, D. P. 1990, *ApJ*, 365, 544
- Brodie, J. P., & Strader, J. 2006, *ARA&A*, 44, 193
- Combes, F., Leon, S., & Meylan, G. 1999, *A&A*, 352, 149
- Cox, T. J., & Loeb, A. 2008, *MNRAS*, 386, 461
- Cresci, G., Vanzi, L., & Sauvage, M. 2005, *A&A*, 433, 447
- Dale, J. E., Bonnell, I. A., Clarke, C. J., & Bate, M. R. 2005, *MNRAS*, 358, 291
- Davis, M., Efstathiou, G., Frenk, C. S., & White, S. D. M. 1985, *ApJ*, 292, 371
- de Grijs, R. 2007, *ArXiv e-prints*
- Elmegreen, B. G. 1989, *ApJ*, 338, 178
- . 2011, *ApJ*, 731, 61
- Elmegreen, B. G., & Efremov, Y. N. 1997, *ApJ*, 480, 235
- Fall, S. M., & Chandar, R. 2012, *ApJ*, 752, 96
- Fall, S. M., & Rees, M. J. 1985, *ApJ*, 298, 18

- Fall, S. M., & Zhang, Q. 2001, *ApJ*, 561, 751
- Feng, Y., Croft, R. A. C., Di Matteo, T., & Khandai, N. 2013, *MNRAS*, 429, 1554
- Forbes, D. A., & Bridges, T. 2010, *MNRAS*, 404, 1203
- Gieles, M., & Baumgardt, H. 2008, *MNRAS*, 389, L28
- Gill, S. P. D., Knebe, A., & Gibson, B. K. 2004, *MNRAS*, 351, 399
- Gingold, R. A., & Monaghan, J. J. 1977, *MNRAS*, 181, 375
- Gnedin, O. Y., Hernquist, L., & Ostriker, J. P. 1999a, *ApJ*, 514, 109
- Gnedin, O. Y., Lee, H. M., & Ostriker, J. P. 1999b, *ApJ*, 522, 935
- Gnedin, O. Y., & Ostriker, J. P. 1997, *ApJ*, 474, 223
- Goddard, Q. E., Bastian, N., & Kennicutt, R. C. 2010, *MNRAS*, 405, 857
- Gratton, R. G., Carretta, E., & Bragaglia, A. 2012, *A&A Rv*, 20, 50
- Haardt, F., & Madau, P. 1996, *ApJ*, 461, 20
- Harris, W. E. 1991, *ARA&A*, 29, 543
- Harris, W. E. 2001, in *Saas-Fee Advanced Course 28: Star Clusters*, ed. L. Labhardt & B. Binggeli, 223
- Hayward, C. C., Torrey, P., Springel, V., Hernquist, L., & Vogelsberger, M. 2014, *MNRAS*, 442, 1992
- Hernquist, L. 1989, *Nature*, 340, 687
- . 1990, *ApJ*, 356, 359
- Hernquist, L., & Katz, N. 1989, *ApJS*, 70, 419
- Herrera, C. N., Boulanger, F., & Nesvadba, N. P. H. 2011, *A&A*, 534, A138
- Holtzman, J. A., Faber, S. M., Shaya, E. J., Lauer, T. R., Groth, J., Hunter, D. A., Baum, W. A., Ewald, S. P., Hester, J. J., Light, R. M., Lynds, C. R., O'Neil, Jr., E. J., & Westphal, J. A. 1992, *AJ*, 103, 691
- Hopkins, P. F. 2015, *MNRAS*, 450, 53
- Hopkins, P. F., Cox, T. J., Hernquist, L., Narayanan, D., Hayward, C. C., & Murray, N. 2013, *MNRAS*, 430, 1901
- Hopkins, P. F., Cox, T. J., Younger, J. D., & Hernquist, L. 2009, *ApJ*, 691, 1168
- Hopkins, P. F., Hernquist, L., Cox, T. J., Di Matteo, T., Martini, P., Robertson, B., & Springel, V. 2005, *ApJ*, 630, 705
- Hopkins, P. F., Hernquist, L., Cox, T. J., & Kereš, D. 2008, *ApJS*, 175, 356
- Hopkins, P. F., Hernquist, L., Cox, T. J., Robertson, B., & Springel, V. 2006, *ApJS*, 163, 50
- Jenkins, E. B., Jura, M., & Loewenstein, M. 1983, *ApJ*, 270, 88
- Jog, C. J., & Das, M. 1996, *ApJ*, 473, 797
- Jog, C. J., & Solomon, P. M. 1992, *ApJ*, 387, 152
- Johnson, K. E., Leroy, A. K., Indebetouw, R., Brogan, C. L., Whitmore, B. C., Hibbard, J., Sheth, K., & Evans, A. S. 2015, *ApJ*, 806, 35
- Jordán, A., McLaughlin, D. E., Côté, P., Ferrarese, L., Peng, E. W., Mei, S., Villegas, D., Merritt, D., Tonry, J. L., & West, M. J. 2007, *ApJS*, 171, 101
- Kennicutt, Jr., R. C. 1998, *ApJ*, 498, 541
- Kereš, D., Vogelsberger, M., Sijacki, D., Springel, V., & Hernquist, L. 2012, *MNRAS*, 425, 2027
- Keto, E., Ho, L. C., & Lo, K.-Y. 2005, *ApJ*, 635, 1062
- Klypin, A., & Holtzman, J. 1997, *ArXiv Astrophysics e-prints*
- Knierman, K. A., Gallagher, S. C., Charlton, J. C., Hunsberger, S. D., Whitmore, B., Kundu, A., Hibbard, J. E., & Zaritsky, D. 2003, *AJ*, 126, 1227
- Knollmann, S. R., & Knebe, A. 2009, *ApJS*, 182, 608
- Krujijssen, J. M. D. 2014, *Classical and Quantum Gravity*, 31, 244006
- . 2015, *MNRAS*, 454, 1658
- Krujijssen, J. M. D., & Cooper, A. P. 2012, *MNRAS*, 420, 340
- Krujijssen, J. M. D., Pelupessy, F. I., Lamers, H. J. G. L. M., Portegies Zwart, S. F., Bastian, N., & Icke, V. 2012, *MNRAS*, 421, 1927
- Krujijssen, J. M. D., Pelupessy, F. I., Lamers, H. J. G. L. M., Portegies Zwart, S. F., & Icke, V. 2011, *MNRAS*, 414, 1339
- Krumholz, M. R., Bate, M. R., Arce, H. G., Dale, J. E., Gutermuth, R., Klein, R. I., Li, Z.-Y., Nakamura, F., & Zhang, Q. 2014, *Protostars and Planets VI*, 243
- Lamers, H. J. G. L. M., Baumgardt, H., & Gieles, M. 2010, *MNRAS*, 409, 305
- Larsen, S. S. 2010, *Philosophical Transactions of the Royal Society of London Series A*, 368, 867
- Li, Y., Hernquist, L., Robertson, B., Cox, T. J., Hopkins, P. F., Springel, V., Gao, L., Di Matteo, T., Zentner, A. R., Jenkins, A., & Yoshida, N. 2007, *ApJ*, 665, 187
- Li, Y., Mac Low, M.-M., & Klessen, R. S. 2004, *ApJL*, 614, L29
- Longmore, S. N., Krujijssen, J. M. D., Bastian, N., Bally, J., Rathborne, J., Testi, L., Stolte, A., Dale, J., Bressert, E., & Alves, J. 2014, *Protostars and Planets VI*, 291
- Lützgendorf, N., Baumgardt, H., & Krujijssen, J. M. D. 2013, *A&A*, 558, A117
- McCraday, N., & Graham, J. R. 2007, *ApJ*, 663, 844
- McLaughlin, D. E., & Fall, S. M. 2008, *ApJ*, 679, 1272
- Mengel, S., Lehnert, M. D., Thatte, N., & Genzel, R. 2002, *A&A*, 383, 137
- Mengel, S., Lehnert, M. D., Thatte, N. A., Vacca, W. D., Whitmore, B., & Chandar, R. 2008, *A&A*, 489, 1091
- Miah, J. A., Sharples, R. M., & Cho, J. 2015, *MNRAS*, 447, 3639
- Mihos, J. C., & Hernquist, L. 1994, *ApJL*, 431, L9
- . 1996, *ApJ*, 464, 641
- Miller, B. W., Whitmore, B. C., Schweizer, F., & Fall, S. M. 1997, *AJ*, 114, 2381
- Mistani, P. A., Sales, L. V., Pillepich, A., Sanchez-Janssen, R., Vogelsberger, M., Nelson, D., Rodriguez-Gomez, V., Torrey, P., & Hernquist, L. 2016, *MNRAS*, 455, 2323
- Mo, H. J., Mao, S., & White, S. D. M. 1998, *MNRAS*, 295, 319
- Mullan, B., Konstantopoulos, I. S., Kephley, A. A., Lee, K. H., Charlton, J. C., Knierman, K., Bastian, N., Chandar, R., Durrell, P. R., Elmegreen, D., English, J., Gallagher, S. C., Gronwall, C., Hibbard, J. E., Hunsberger, S., Johnson, K. E., Maybhate, A., Palma, C., Trancho, G., & Vacca, W. D. 2011, *ApJ*, 731, 93
- Nelson, D., Vogelsberger, M., Genel, S., Sijacki, D., Kereš, D., Springel, V., & Hernquist, L. 2013, *MNRAS*, 429, 3353
- Parmentier, G., & Gilmore, G. 2007, *MNRAS*, 377, 352
- Portegies Zwart, S. F., McMillan, S. L. W., & Gieles, M. 2010, *ARA&A*, 48, 431
- Prieto, J. L., & Gnedin, O. Y. 2008, *ApJ*, 689, 919
- Renaud, F. 2010, *PhD thesis*, PhD Thesis, 281 pages, 121 figures, 2010
- Renaud, F., Boily, C. M., Naab, T., & Theis, C. 2009, *ApJ*, 706, 67
- Renaud, F., Bournaud, F., & Duc, P.-A. 2015, *MNRAS*, 446, 2038
- Renaud, F., Bournaud, F., Kraljic, K., & Duc, P.-A. 2014, *MNRAS*, 442, L33
- Renaud, F., & Gieles, M. 2013, *MNRAS*, 431, L83
- Renaud, F., Gieles, M., & Boily, C. M. 2011, *MNRAS*, 418, 759
- Rodriguez-Gomez, V., Genel, S., Vogelsberger, M., Sijacki, D., Pillepich, A., Sales, L. V., Torrey, P., Snyder, G., Nelson, D., Springel, V., Ma, C.-P., & Hernquist, L. 2015, *MNRAS*, 449, 49
- Schaye, J., Crain, R. A., Bower, R. G., Furlong, M., Schaller, M., Theuns, T., Dalla Vecchia, C., Frenk, C. S., McCarthy, I. G., Helly, J. C., Jenkins, A., Rosas-Guevara, Y. M., White, S. D. M., Baes, M., Booth, C. M., Camps, P., Navarro, J. F., Qu, Y., Rahmati, A., Sawala, T., Thomas, P. A., & Trayford, J. 2015, *MNRAS*, 446, 521
- Schmidt, M. 1959, *ApJ*, 129, 243

- Schweizer, F., Miller, B. W., Whitmore, B. C., & Fall, S. M. 1996, *AJ*, 112, 1839
- Scoville, N. Z., Yun, M. S., & Bryant, P. M. 1997, *ApJ*, 484, 702
- Sijacki, D., Vogelsberger, M., Kereš, D., Springel, V., & Hernquist, L. 2012, *MNRAS*, 424, 2999
- Springel, V. 2000, *MNRAS*, 312, 859
- 2005, *MNRAS*, 364, 1105
- Springel, V., Di Matteo, T., & Hernquist, L. 2005a, *MNRAS*, 361, 776
- Springel, V., & Hernquist, L. 2002, *MNRAS*, 333, 649
- 2003a, *MNRAS*, 339, 289
- 2003b, *MNRAS*, 339, 312
- 2005, *ApJL*, 622, L9
- Springel, V., White, S. D. M., Jenkins, A., Frenk, C. S., Yoshida, N., Gao, L., Navarro, J., Thacker, R., Croton, D., Helly, J., Peacock, J. A., Cole, S., Thomas, P., Couchman, H., Evrard, A., Colberg, J., & Pearce, F. 2005b, *Nature*, 435, 629
- Springel, V., Yoshida, N., & White, S. D. M. 2001, *NewA*, 6, 79
- Suginohara, T., & Suto, Y. 1992, *ApJ*, 387, 431
- Thrall, H. 2008, in *Astronomical Society of the Pacific Conference Series*, Vol. 390, *Pathways Through an Eclectic Universe*, ed. J. H. Knapen, T. J. Mahoney, & A. Vazdekis, 200
- VandenBerg, D. A., Brogaard, K., Leaman, R., & Casagrande, L. 2013, *ApJ*, 775, 134
- Varenus, E., Conway, J. E., Martí-Vidal, I., Aalto, S., Barcos-Muñoz, L., König, S., Pérez-Torres, M. A., Deller, A. T., Moldón, J., Gallagher, J. S., Yoast-Hull, T. M., Horellou, C., Morabito, L. K., Alberdi, A., Jackson, N., Beswick, R., Carozzi, T. D., Wucknitz, O., & Ramírez-Olivencia, N. 2016, *A&A*, 593, A86
- Vesperini, E. 2000, *MNRAS*, 318, 841
- 2001, *MNRAS*, 322, 247
- Vesperini, E., & Heggie, D. C. 1997, *MNRAS*, 289, 898
- Vogelsberger, M., Sijacki, D., Kereš, D., Springel, V., & Hernquist, L. 2012, *MNRAS*, 425, 3024
- Warren, M. S., Quinn, P. J., Salmon, J. K., & Zurek, W. H. 1992, *ApJ*, 399, 405
- Webb, J. J., & Leigh, N. W. C. 2015, *MNRAS*, 453, 3278
- Wei, L. H., Keto, E., & Ho, L. C. 2012, *ApJ*, 750, 136
- Welty, D. E., Lauroesch, J. T., Wong, T., & York, D. G. 2016, *ApJ*, 821, 118
- Whitmore, B. C., Chandar, R., Schweizer, F., Rothberg, B., Leitherer, C., Rieke, M., Rieke, G., Blair, W. P., Mengel, S., & Alonso-Herrero, A. 2010, *AJ*, 140, 75
- Whitmore, B. C., & Schweizer, F. 1995, *AJ*, 109, 960
- Whitmore, B. C., Schweizer, F., Leitherer, C., Borne, K., & Robert, C. 1993, *AJ*, 106, 1354
- Whitmore, B. C., Zhang, Q., Leitherer, C., Fall, S. M., Schweizer, F., & Miller, B. W. 1999, *AJ*, 118, 1551
- Zhang, H.-X., Gao, Y., & Kong, X. 2010, *MNRAS*, 401, 1839
- Zhang, Q., & Fall, S. M. 1999, *ApJL*, 527, L81
- Zhu, Q., Hernquist, L., & Li, Y. 2015, *ApJ*, 800, 6
- Zhu, Q., & Li, Y. 2016, *ArXiv* 1606.00796
- Zubovas, K., Sabulis, K., & Naujalis, R. 2014, *MNRAS*, 442, 2837